Article

Fabrication and *In Vitro* Drug Delivery Evaluation of Cephalexin Monohydrate-Loaded PLA:PVA/HAP:TiO₂ Fibrous Scaffolds for Bone Regeneration

Rama Murugapandian, Simona Clement, and Vijayalakshmi Uthirapathy*

Read Online

ACCESS | Metrics & More | Article Recommendations

ABSTRACT: Owing to the excellent osteoconductive property of hydroxyapatite, we aimed to design a cephalexin monohydrate-loaded PLA:PVA/HAP:TiO₂ nanofibrous scaffold to improve the drug delivery efficiency toward bone regenerative applications. In this study, HAP:TiO₂ (anatase and rutile phases) samples were prepared by a coprecipitation method, which were later blended with PLA:PVA polymeric solution (with and without the drug) to fabricate a nanofibrous matrix via the electrospinning technique. All the prepared samples were characterized by Fourier transform infrared spectroscopy, X-ray diffraction, scanning electron microscopy, contact angle, porosity, and tensile strength tests. Further, *in vitro* biodegradation and the drug-releasing ability were examined by varying the concentration of cephalexin monohydrate in the composite matrix. Deposition of the apatite layer on the scaffolds was examined after incubation in simulated body fluid solution to confirm the bioactivity of the prepared nanofibers. Biocompatibility by the MTT assay and osteogenic differentiation by ARS staining were evaluated by culturing MG63 cells on PLA:PVA/HAP:TiO₂ nanofibers, which could ensue better support for cell proliferation. Consequently, the sustained release profile and better biocompatibility of the scaffolds revealed a strong potential use in bone regenerative applications.
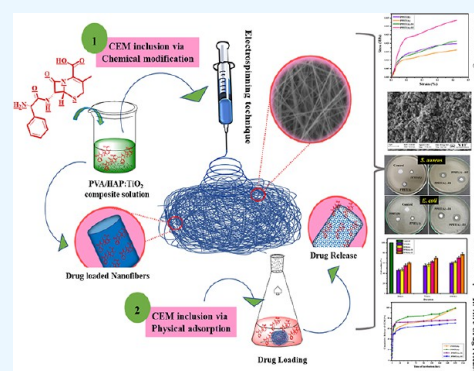
■ HIGHLIGHTS

- Antibiotic drug-embedded anatase- and rutile-phase TiO₂/HAP nanofibrous scaffolds were successfully fabricated using an electrospinning technique.
- Antibiotic drug CEM-loaded PLA:PVA/HAP:TiO₂ electrospun nanofibrous scaffolds revealed a better sustained release and antibacterial efficacy, and osteogenic differentiation was examined by ARS staining.
- The mechanical study, hemocompatibility assay, and cell viability assessment were compared and interpreted for effective use of the prepared nanofibers in bone regenerative applications.
- The incorporation of CEM in spinning solution forms strong covalent linkages that can enhance better releasing progress than the scaffolds loaded via physical adsorption.

1. INTRODUCTION

Bone is a dynamic rigid organ that undergoes remodeling processes over a lifetime and sometimes becomes intricate due to bone-related disorders, which are caused by bone diseases, high energy injuries, or pathological fracture.[1] Around $45 billion is being utilized for conventional treatments toward bone healing, which are still impaired due to the age factor and surgeries that impede the quality of life.[2] Autografting is an exclusive method that is considered as a "gold standard" to treat bone tissue regeneration, although limited due to its immunogenic reaction, donor availability, etc. Bone tissue engineering (BTE) is an interdisciplinary vital phenomenon that focuses on 3D structures named "scaffolds or biological substitutes" to mimic the extracellular matrix (ECM) to improve tissue functions or reconstruction.[3] Scaffolds possess inherent capacity that promotes cellular-level functions such as cell stimulation, adhesion, and proliferation and give a mechanical support for tissue ingrowth/ regeneration. The intention of the desired scaffold is to (i) enhance osteoinduction (inducing cell differentiation to support bone growth), (ii) induce an osteoconductive property (ability to form new bones), and (iii) stimulate osseointegration (integration to surrounding tissues).[4] Recently, numerous bioinspired drug-embedded scaffolds are designed and fabricated to stimulate the biological activity toward cell

regeneration. Fathi *et al.* reported that systematic drug treatment via oral administration or by injection could lower the efficacy of a drug at the area of its applications, whereas drug release by the implant could avoid bacterial concentration.[5]

Hydroxyapatite (HAP), a calcium phosphate bioceramic, bears chemical, biological, and structural similarities to the natural bone extracellular matrix (ECM, a biological apatite structure bounded with an organic matrix). It has excellent chemical compatibility with bones, osteoinductive property, and low toxicity and acts as a drug carrier to reduce bone infections.[6] Though HAP supports osteoblastic cell growth, the main drawback is low mechanical strength due to its brittleness, which limits its use in biomedical applications.[7] Titanium dioxide (TiO_2) has a polymorphic nature that is exhibited in two main crystalline phases (anatase and rutile) with a photocatalytic activity that could inhibit bacterial colonization. It is used in various applications including dental/orthopedic industries for coatings on metallic implants to resist corrosion.[8] Khan *et al.* reported that the addition of TiO_2 in the HAP composite increased the mechanical and biological property.[9] Similarly, Stipniece *et al.* reported that the metabolic activity (*i.e.*, cell viability and cytostatic activity) increased upon the addition of HAP into the TiO_2/PVA composite.[10] Hence, the combination of TiO_2 and HAP in the composite could increase the osseointegration and mechanical performance to enhance the bone regeneration[11] and drug delivery ability of the composite.

Electrospinning is an excellent technique for producing ultrathin fibers in the form of nanofibrous scaffolds (ranging from 50 to 1000 nm or even greater) with a high surface area.[12] The parameters such as viscosity, molecular weight of the polymer, conductivity, flow rate, composition, temperature, and humidity are the factors that could affect the fabrication of scaffolds using the electrospinning technique.[13,14] In addition, an electrospun (espun) nanofibrous scaffold favors *in vivo* cell interactions and delivery of therapeutic drugs/proteins/genes/growth factors and thereby stimulates bone ingrowth. PLA (polylactic acid) is a hydrophobic polyester, which has been widely used in tissue engineering, drug delivery, and surgical sutures.[15] Biocompatible PLA nanofibers have interconnected pores with a high surface area, which could serve as a better drug delivery carrier.[16] PVA (polyvinyl alcohol) is a synthetic semicrystalline biodegradable polymer that is known for its hydrophilicity, biocompatibility and nontoxicity, thermal characteristics, processability, and gas permeability.[17,18] However, PVA is used to overcome the poor mechanical property and hydrophobicity of PLA.

Pereira *et al.* reported that the "enhanced permeability and retention" (EPR) effect coined by Maeda and Matsumura could decrease the side effects of a drug and improve the efficacy, where the drug is homogeneously distributed in the polymeric matrix. The study suggested that chemical conjugation of the drug in the matrix could minimize the systematic toxicity and improves *in vivo* stability and bioavailability of the drug.[19] Cephalexin monohydrate (CEM, an antibacterial drug having similar functional groups to penicillin) contains beta-lactam and dihydrothiazide,[20] an innocuous antibiotic used to treat a large number of bacterial infections related to bones, respiratory tracts, skin infections, etc.[21] Kataria *et al.* reported that the cephalexin drug loaded (during electrospinning) into PVA nanofibers showed burst release (almost 98.7% drug released in 7 h) due to the drug

attached on the surface. The study anticipated that strong interactions between biocompatible CEM and the composite nanofiber could increase the *in vivo* antibacterial effect over 20 days.[22] Drug inclusion via the chemical method can reduce burst release and result in prolonged drug release from the polymeric scaffold.[23]

In this work, we report a flexible bioactive drug-loaded nanofibrous scaffold by blending different concentrations of CEM into spinning solutions for fabrication. PLA:PVA/HAP:TiO_2/CEM nanofibrous scaffolds could provide an ideal microenvironment for cell migration and proliferation and enhance the prolonged antibacterial effect. The inclusion of a drug by chemical modification via blending of the drug with spinning solution and inclusion of a drug via physical adsorption were attempted, and the efficacy of release was compared in detail.

2. EXPERIMENTAL METHODS

2.1. Synthesis of Nano-HAP and TiO_2. HAP was prepared using a coprecipitation method by dissolving the aqueous solution of 0.6 M ammonium dihydrogen orthophosphate ($NH_4H_2PO_4$, from SDFCL Fine-Chem Limited, India) and 1 M calcium nitrate tetrahydrate ($Ca(NO_3)_2 \cdot 4H_2O$, from SDFCL Fine-Chem Limited, India). Ammonia was added to the reaction mixture until the pH reached 10. The slurry solution was stirred at 600 RPM and kept for aging overnight under ambient temperature. Subsequently, the obtained precipitate was filtered and washed with distilled water. Finally, the powder was dried and calcined at 900 °C for 2 h.

TiO_2 was synthesized by mixing titanium tetraisopropoxide (AVRA Synthesis Private Limited, India), with acetic acid and deionized water at a molar ratio of 1:30:300. This mixture was stirred at 630 RPM for 2 h and subsequently refluxed in an oil bath at 90 °C overnight. The resultant solution was evaporated in a water bath and dried, and the crystalline powder was further ground, sintered at 550 °C for 2 h to acquire anatase, and sintered at 1000 °C to obtain the rutile phase of TiO_2. Finally, the obtained powder was ball-milled with HAP in a weight ratio of 3:2 (3 wt % HAP, 2 wt % TiO_2) and dried.

2.2. Preparation of Electrospinning Solution. The electrospun nanofibers are labeled in Table 1 along with the

Table 1. Fabrication of Electrospun HAP:TiO_2-Based Nanofibers

solution	composition	label of the nanofiber
A	PLA:PVA/HAP:$TiO_{2(rutile)}$	PPHT(R)
B	PLA:PVA/HAP:$TiO_{2(anatase)}$	PPHT(A)
C	PLA:PVA/HAP:$TiO_{2(anatase)}$/D1 (2.5 mg/mL)	PPHT(A)-D1
D	PLA:PVA/HAP:$TiO_{2(anatase)}$/D2 (5 mg/mL)	PPHT(A)-D2

composition. In brief, solutions A and B were prepared by dissolving HAP:TiO_2 (anatase and rutile) in 10% of the PLA:PVA solution. To this spinning solution A (*i.e.*, HAP:TiO_2 (anatase)/PLA:PVA), the CEM drug was added in concentrations of 2.5 (D1) and 5 mg/mL (D2). The prepared solutions were stirred overnight at room temperature to obtain homogeneity. Finally, nanofibers were obtained using an electrospinning instrument (ESPIN, Nano, Physics Equipments) at an applied voltage of 19 kV with a flow rate of 1 mL/

h. The collector−tip distance was kept at 12−15 cm, and the rotational speed was set at 700 RPM.

3. ANALYTICAL METHODS

3.1. Characterization Techniques. Prepared HAP, TiO$_2$ particles, and electrospun nanofibers were characterized using a Fourier transform infrared spectrometer (FTIR: IR Affinity-1 SHIMADZU), an X-ray diffractometer (SHIMADZU XRD-600), and a scanning electron microscope (FE-SEM: JEOL 200CX operated at 200 kV). The tensile strength of the scaffold was measured using an ASTM standard (D695) on a Tinus Olsen H5K5 universal testing machine. The nanofibers with a 0.10−0.12 mm thickness and a height of 6 cm were fixed between two clamps bearing 5000 N, and the average of triplicates was calculated by plotting the obtained stress−strain curves to minimize the error.

3.2. *In Vitro* Biomineralization Assessment. The bioactivity of the scaffolds in terms of apatite formation on the scaffold surface was evaluated in a simulated body fluid (SBF) for 14 days at 37 °C. After incubation periods, the samples were washed, rinsed, and the dried in an oven at 60 °C for 24 h. Morphological changes were examined using SEM, FTIR, and XRD analysis.

3.3. *In Vitro* Degradation and Porosity Measurement. *In vitro* degradation investigation of CEM-loaded PLA:PVA/HAP:TiO$_2$ nanofibers was estimated using SBF solution (Hank's solution) at pH 7.4 without any enzymes. The scaffolds were immersed in 20 mL of SBF solution for 28 days; then, immersed scaffolds were gently rinsed in distilled water, dehydrated at 60 °C, and weighed. The weight loss of the scaffolds (rate of degradation) was computed using the following formula (Hu *et al.*):[24]

$$\text{weight loss of the scaffold } (\%) = \frac{(W_i - W_f)}{W_i} \times 100$$

where W_i is the initial dry weight of the scaffold and W_f is the final dry weight of the scaffold after immersion.

The porosity (ε) of the CEM-loaded HAP/TiO$_2$ nanofibers was measured by the solvent replacement method using absolute ethanol as per our previous protocol.[25] In detail, the square-shaped PLA:PVA/HAP:TiO$_2$ nanofibers were immersed in ethanol (V) for 48 h until saturation was complete and weight measurements were recorded. The air-dried scaffolds were weighed to estimate the porosity of the nanofibers based on the mathematical formula as follows:

$$\text{porosity } (\%) = \frac{M2 - M1}{\rho V} \times 100$$

where $M1$ is the mass of the nanofibers weighed before immersion, $M2$ is the saturated wet weight after immersion in absolute ethanol, ρ is the density of ethanol, and V is the volume of the nanofiber.

3.4. Antibacterial Evaluation and Blood Compatibility Analysis. The antibacterial test was evaluated based on our previous protocol[26] using a disc diffusion test and a CFU study against Gram-positive *Staphylococcus aureus* (*S. aureus*) and Gram-negative *Escherichia coli* (*E. coli*) and *Bacillus subtilis* for wound infection and regeneration processes. The drug-embedded fibrous scaffolds were cut into a disc shape and sterilized by ultraviolet radiation for 30 min before the studies. For qualitative analysis, the pathogens were cultured uniformly over Petri plates in agar medium via a spread plate technique.

The sterilized discs were placed in agar and incubated for 24 h at 37 °C, and the area of inhibition zones was imaged by a digital camera to elucidate the bactericidal effect of the samples. For quantitative analysis, the test extracts of the scaffolds were prepared in sterilized physiological saline incubating the same at body temperature (37 °C) for 6 h. Post incubation, the test extract was collected in sterilized vials and treated with an equal quantity of serially diluted bacterial culture and incubated for 2 h in a CO$_2$ incubator. About 0.1 mL of the test extract was inoculated with bacteria over sterilized nutrient agar media plates using the standard spread plate method for 24 h in a CO$_2$ incubator. The average number of CFUs was further calculated using a digital colony counter, and respective quantitative values were calculated according to the following equation.[26]

$$\frac{\text{number of colonies obtained} \times \text{dilution factor}}{\text{volume of sample plated}}$$

The blood compatibility of the flax:silk fibroin electrospun nanofibers was evaluated by the hemolysis assay (ASTM F 756-00 guidelines). In brief, human red blood cells were separated from plasma, and the scaffolds were sterilized in physiological saline at normal body temperature. About 20 μL of diluted blood (20 μL of fresh anticoagulant blood in 10 mL of 0.9% saline) was dropped into 5 mL sample vials containing 1 mg of composite nanofibers. Samples were incubated for 60 min at 37 °C and centrifuged at 2500 RPM for 10 min. The hemolytic percentage was determined by taking the supernatant using UV−visible scanning spectrophotometer analysis (Shimadzu UV-1800), and the values were recorded at a wavelength of 545 nm. The hemolysis ratio (HR) was calculated as follows:[27]

$$\text{HR} = \frac{\text{Dt} - \text{Dnc}}{\text{Dpc} - \text{Dnc}} \times 100\%$$

where HR is the hemolysis ratio and Dt, Dnc, and Dpc are average absorbance values of the respective sample, negative control (saline), and positive control (distilled water), respectively. Hemolytic grades were determined as nonhemolytic for HR values between 0 and 2, with 2−5 as slightly hemolytic and hemolytic for above 5 units.

3.5. *In Vitro* Cell Viability by the MTT Assay and Osteogenic Differentiation by ARS Staining Using MG63 Cells. A standard MTT assay was used to analyze the cell viability of the prepared CEM-loaded PLA:PVA/HAP:TiO$_2$ nanofibers. The nanofibers were examined using the MG63 human osteoblast cell line using 96-well plates with a concentration of 1×10^4 cells/well in DMEM media with 1× antibiotic−antimycotic solution and 10% fetal bovine serum (FBS, Himedia, India) in a controlled atmosphere (5% CO$_2$, T = 37 °C). The cells were washed with 200 μL of 1× PBS, and then, the cells were treated with various test concentrations of the synthesized CEM-loaded PLA:PVA/HAP:TiO$_2$ nanocomposite materials in serum-free media and kept for incubation for a duration of 24 h. The conditions of each culture were monitored every single day, and the medium was aspirated from cells at the end of the treatment period. MTT solution at a concentration of 0.5 mg/mL was then added and further incubated for 3−4 h. Subsequently, the medium containing MTT was discarded from the cells and washed using 200 μL of PBS. The absorbance of each well was
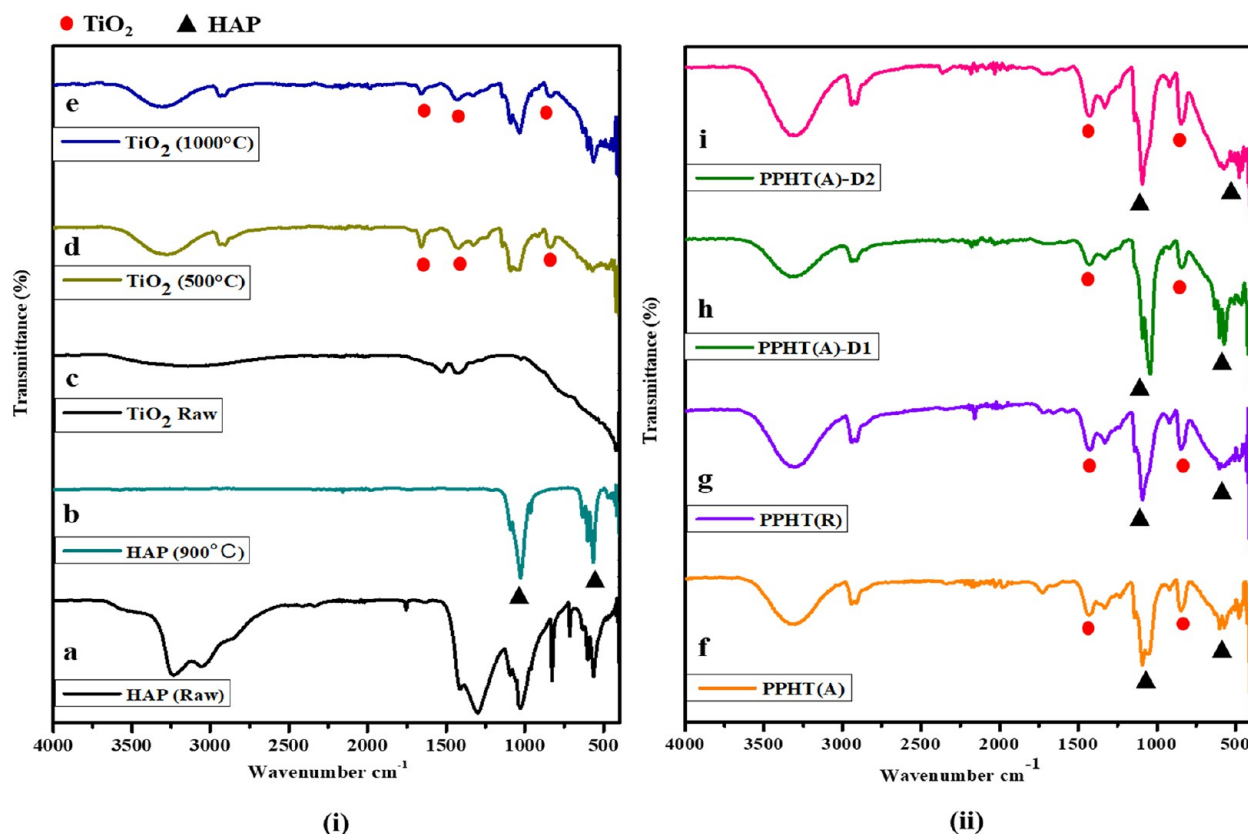
Figure 1. FTIR spectra of as-synthesized HAP and TiO_2 with different sintering temperatures (i) and espun PLA:PVA/HAP:TiO_2 nanofibers with and without CEM (ii).

measured at 570 nm using a spectrophotometer for 28, 72, and 198 h.

The formation of calcium nodules by MG63 osteoblast-like cells on the nanofibers was evaluated by the Alizarin red staining (ARS) method. In brief, MG63 cells were seeded on the scaffolds (24-well plate) and cultured for 14 days. After 14 days of inoculation, the scaffolds were washed three times with PBS and fixed with 4% paraformaldehyde for 1 h at room temperature. Later, the seeded scaffolds were washed and stained using 1% ARS solution (pH 4.1−4.3); then, the scaffolds were washed to remove excess dye and photographed with a microscope.

3.6. Drug Loading and Release Efficacy of the Scaffolds. The CEM loading and release from scaffolds were investigated by two different methods, *i.e.*, drug release from CEM-loaded PLA:PVA/HAP:TiO_2 (anatase and rutile) nanofibers and drug release from CEM-incorporated HAP:-TiO_2 (anatase)/PLA:PVA spinning solution by varying the drug concentration (2.5 and 5 mg/mL) to evaluate the release profile. In addition, CEM was loaded in rutile and anatase PPHT nanofibers by cutting them into 2×2 cm^2 and immersed in the cephalexin drug (50 mL) via physical adsorption. The loaded nanofibers were then released in an orbital shaker with constant shaking at 60 RPM. The loading efficacy and cumulative release were calculated by taking a UV−visible spectrophotometer (model no. UV 3092 Lab India Analytical Instruments) in predetermined intervals (0, 0.5, 1, 1.5, 2, 4, 6, 12, and 24 h and continued up to 8 days).

4. RESULTS AND DISCUSSION

4.1. FTIR Analysis. The functional groups of synthesized HAP and TiO_2 powders in various nanofibrous composites were confirmed using FTIR spectroscopy. Figure 1(i)a,b presents HAP with and without sintering at 900 °C. From the figure, it was observed that the band at 550−558 cm^{-1} was attributed to the presence of the P−O−P bending mode in PO_4^{3-} and the asymmetric bending mode of PO_4^{3-} observed at 598 cm^{-1}.[28] The bands at 956 and 1017 cm^{-1} are due to the presence of v_1 symmetric and v_3 asymmetric stretching of P−O in PO_4^{3-}, respectively.[29] The phosphate peak ascribed to HAP was clearly observed in the fabricated sheet, which confirms the incorporation of HAP particles in the scaffold (Figure 1(ii)). The extensive peak of TiO_2 and PLA:PVA polymeric groups was found at 3400 cm^{-1} corresponding to OH stretching vibrations. Figure 1(i)c−e indicates the as-synthesized TiO_2 powders sintered at 500 and 1000 °C. The peaks at 1370, 1634, and 1656 cm^{-1} (in curves d−i) represent the Ti−O stretching, Ti−OH bending, and C=O stretching vibrations. Also, the broad and intense peak below 1087 cm^{-1} and the peak at 780 cm^{-1} are due to the presence of Ti−O−Ti and Ti−O bonds in tetrahedral TiO_2.[30] The fabricated sheets having the composition PLA:PVA/HAP:TiO_2 had peaks at 2936, 853, 1423, and 3300 cm^{-1} corresponding to the asymmetric stretching of CH_2 of PVA, C−C stretching in PLA, CH−OH stretching in HAP, and O−H stretching vibrations, respectively. The sheet with different compositions of the CEM drug in the PLA:PVA/HAP:TiO_2 nanofibers (PPHT(A)-D_1 and PPHT(A)-D_2) had peaks at 592, 853, 3319, and 2936 cm^{-1} representing the PO_4^{3-} symmetric stretching in HAP, C−C stretching in polymer PLA, aromatic
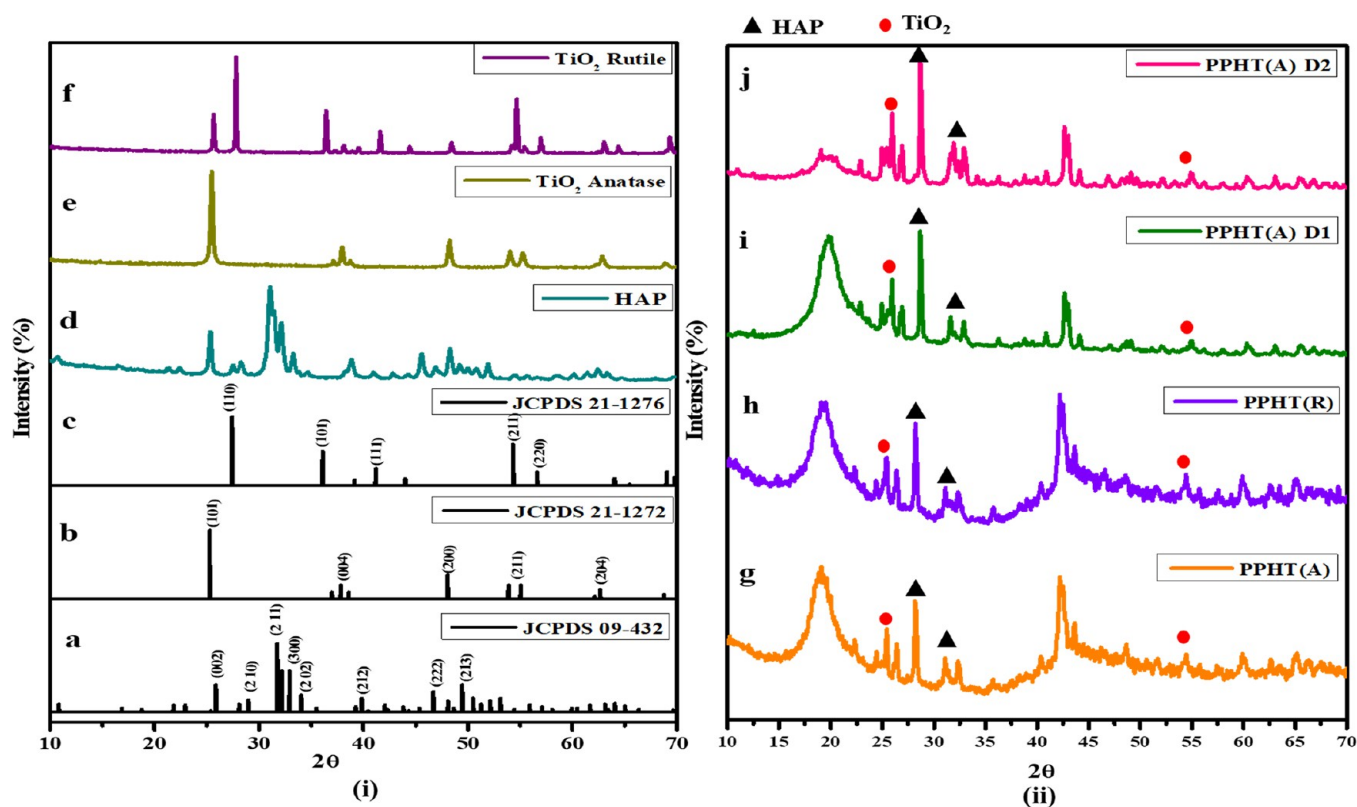
Figure 2. XRD patterns of synthesized HAP and TiO_2 phases (i) and espun PLA:PVA/HAP:TiO_2 nanofibers with and without CEM (ii).

C−H stretching in the drug CEM, and asymmetric stretching of CH_2 in the polymer PVA, respectively. Hence, from Figure 1(i,ii), it was observed that the respective peaks corresponding to HAP and TiO_2 along with the polymeric functional groups are identified.

4.2. XRD Analysis. Figure 2(i)d displays the XRD patterns of HAP sintered at 900 °C and (Figure 2(i)e) TiO_2 powder phases at 500 and (Figure 2(i)f) 1000 °C for 2 h. Figure 2(ii)g−j shows the XRD patterns of PPHTR, PPHTA, and CEM-loaded PPHT(A)-D1 and PPHT(A)-D2 in PLA:PVA/HAP:TiO_2 composite nanofibers. The prominent characteristic peak of HAP was observed at $2\theta = 31.2°$, where the diffraction peaks match with the reference data (Figure 2(i)a, JCPDS 04-932). The peak at 38° corresponding to the anatase $TiO_2(004)$ reflection and the peaks at 25.4, 54, and 63° corresponding to the (101), (211), and (204) refection planes (Figure 2(i)b, JCPDS 21-1272) are clearly observed in the spectra.[31] The intensity peak of rutile TiO_2 (Figure 2(i)c, JCPDS 21-1276) was located at 27.45° corresponding to the (110) plane along with the peaks at 36.5, 63.2, 57, and 54.5° corresponding to *hkl* values of (101), (310), (220), and (211), respectively.[32] The phase transformation of raw TiO_2 powder (as shown in Figure 2(i)) was confirmed with ICDD file no. 21-1272 (tetragonal anatase phase) and ICDD file no. 21-1276 (tetragonal rutile phase). Lukong *et al.* suggested that the phase formation of TiO_2 (*i.e.*, anatase to rutile) and its crystal structure ensues only due to longer annealing times from 600 to 1000 °C.[33]

The fabricated nanofibers (Figure 2(ii)g−j) have a broad peak at 19.2°, which was associated to PVA.[34] A distinctive peak at 25.4° corresponding to the (101) reflection plane confirms the anatase phase of TiO_2 in PPHT(A) nanofibers, whereas peaks at 19, 28, 28.3, and 31.1° correspond to the rutile phase of TiO_2 in PPHT(R). A sharp peak at 28.1°

corresponding to PLA and at 31.2° corresponding to HAP was present in all the nanofibers.[35] The other peaks at 19.6, 22.5, 28.6, 31.6, and 22.5−22.9° indicate the 2θ values of PVA, PLA, HAP, and cephalexin monohydrate for the composite PLA:PVA/HAP:TiO_2-D_1 and PLA:PVA/HAP:TiO_2-D2 sheets (Figure 2(ii)h,i). Compared with the XRD pattern of powder samples (Figure 2(i)), the XRD pattern of nanofibrous sheets (Figure 2(ii)) showed an amorphous structure due to polymer incorporation.

4.3. Particle Size and Morphology. Figure 3a shows that the particle size of sintered HAP at 900° was found to be in the nanoscale level with an average diameter of about 224.5 ± 0.57 nm, determined using a Nanosizer (Horiba Scientific, SZ 100 model). The surface morphologies of TiO_2 powder sintered at 500 and 1000 °C are shown in Figure 3b(i,ii). The surface of rutile and anatase phases of TiO_2 possesses similar uniformity and agglomerated sphere-like microparticles. Figure 3b(iii,iv) micrographs confirm the nanofibrous structure with randomly dispersed coarsened HAP:TiO_2 in the polymer network. Figure 3b(v) shows less bead formation compared to PPHT(R) and PPHT(A) sheets, and this may be due to the incorporation of the drug, which may increase the conductivity of the electrifying solution. The addition of 5 mg/mL drug concentration into nanofibers increased the conductivity; hence, there are no beads found, and the diameter of the fibers is altered (from 355 ± 71 to 587 ± 22 nm). Similar alteration of spinning solution was observed by Rezk *et al.* in their findings.[36] Haider *et al.* proposed that an increase in conductivity of the spinning solution increases the surface charge and decreases the fiber diameter.[37] The conductivity was governed by electrostatic forces generated by the fluid and the applied electrical charge. However, the incorporation of the
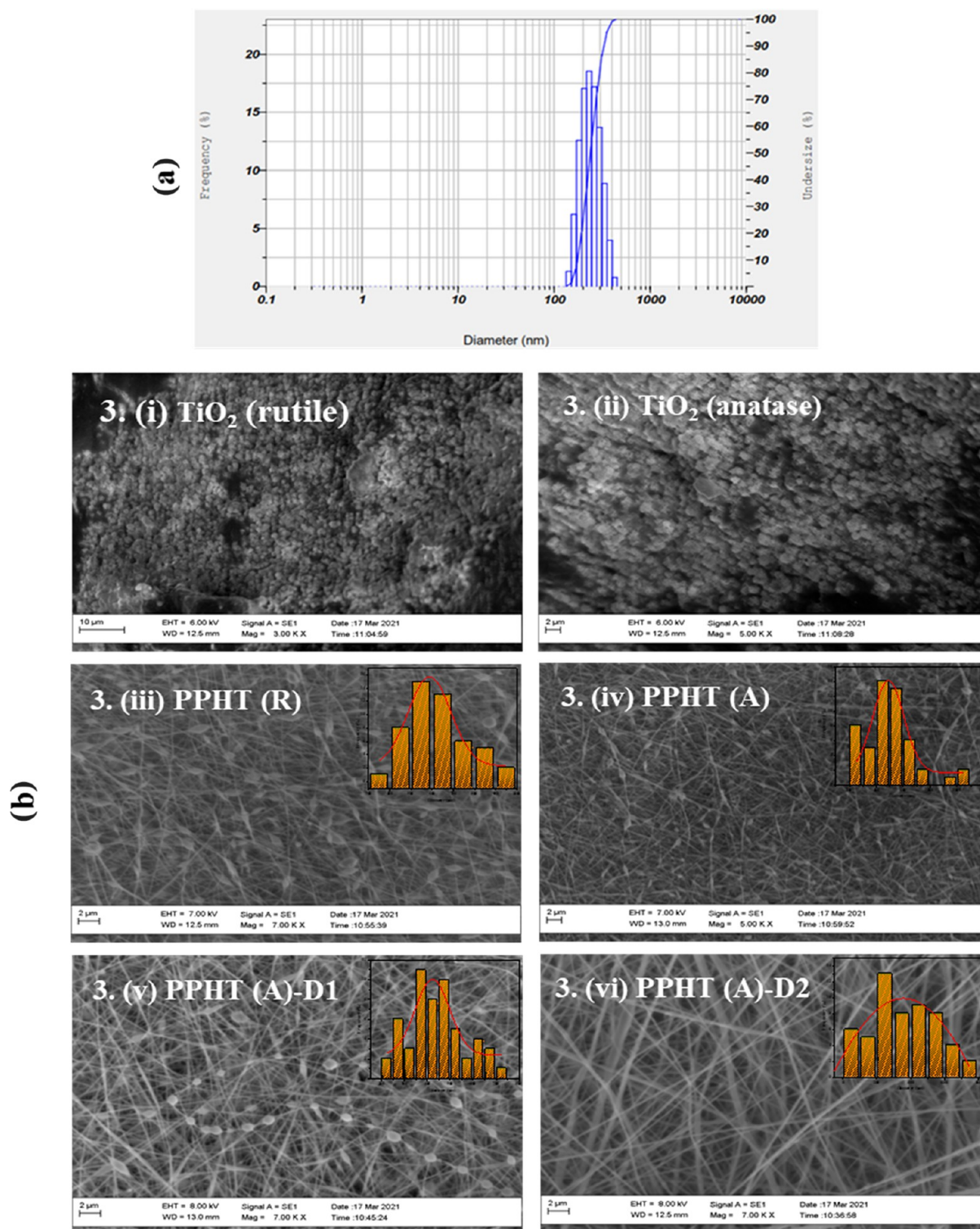
Figure 3. (a) Particle size of synthesized HAP and (b) SEM micrographs of powder TiO_2 (rutile and anatase phase (i,ii)) and espun PLA:PVA/HAP:TiO2 nanofibers with and without CEM (iii,vi).

CEM drug increases the conductivity of the solution and strongly influences the morphology of the nanofibers.

4.4. Water Contact Angle. Incorporation of CEM in the nanofibers may govern the hydrophilic nature where the surface of the nanofibers interacts with macromolecules of the drug. To characterize the water wettability and surface spreading capability, the contact angles of PLA:PVA/HAP:TiO_2 sheets were measured (Figure 4). Though the

degree of contact angles depends upon the water penetration rates and the surface properties of the sheet, HAP in the nanofibers had a nonsignificant impact on hydrophilicity. It was observed that the water contact angle for the rutile TiO_2-based sheet was found to be $27.64 \pm 2.09°$, and the anatase TiO_2-based sheet had a lower contact angle of $17.87 \pm 1.10°$, which is less than that of the rutile sheet. The anatase structure of TiO_2 has a higher energy surface, which favors the
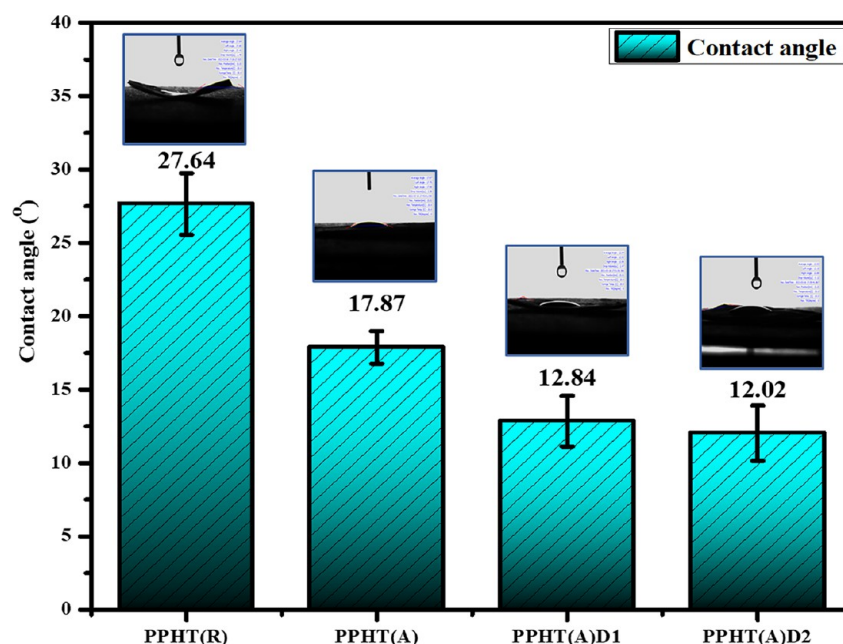
Figure 4. Water contact angles of espun PLA:PVA/HAP:TiO$_2$ nanofibers with and without CEM.
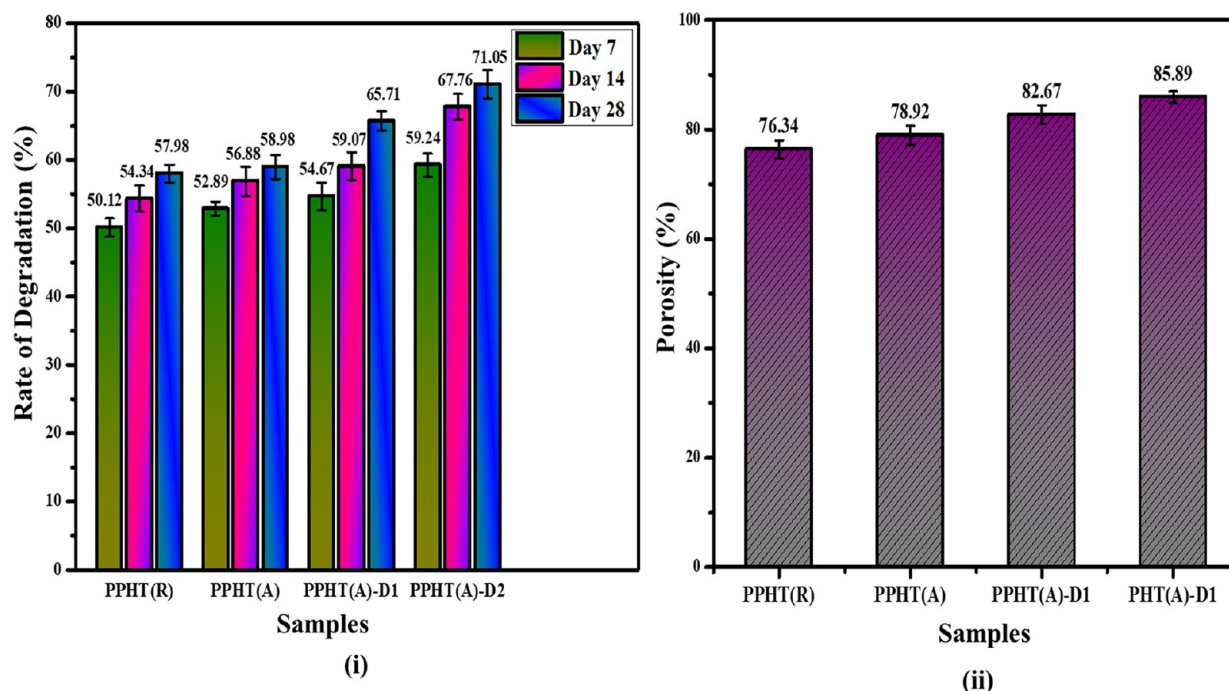

Figure 5. (i) *In vitro* biodegradation of espun PLA:PVA/HAP:TiO$_2$ nanofibers with and without CEM and (ii) porosity of the nanofibers.

adsorption of water and bonds to hydroxyl groups due to surface oxygen vacancies of TiO$_2$. A study by Yu *et al.* anticipated that surface hydroxy groups in the composite could interact with water molecules to form hydrogen bonding and van der Waals bonding, as a result, which increases the hydrophilic nature.[38] Hence, the formation of more hydroxyl groups by TiO$_2$ and hydroxyl groups of PVA in the matrix lowers the contact angle value, resulting in superhydrophilicity. In addition to this content, Niemczyk-Soczynska *et al.* and Cui *et al.* stated that the presence of functional groups such as $-COOH$, $-NH_2$, and $O-H$ bonds facilitates surface hydrophilicity, wherein these groups that were found in the CEM drug favor the surface interactions in the way of enhancing hydrophilicity.[39,40] Cephalexin monohydrate-embedded nanofibers showed contact angles of 12.84 ± 1.72 and 12.02 ± 1.88° corresponding to two different drug concentrations, D1 and D2, respectively. According to Wenzel's and Cassie's theory, the increase in hydrophilicity may be due to the surface roughness, which could also enhance the cell viability and proliferation.[41] Hence, this study further confirms that the presence of strong interactions of CEM and the presence of HAP in the matrix decrease the hydrophobicity of the nanofibers.
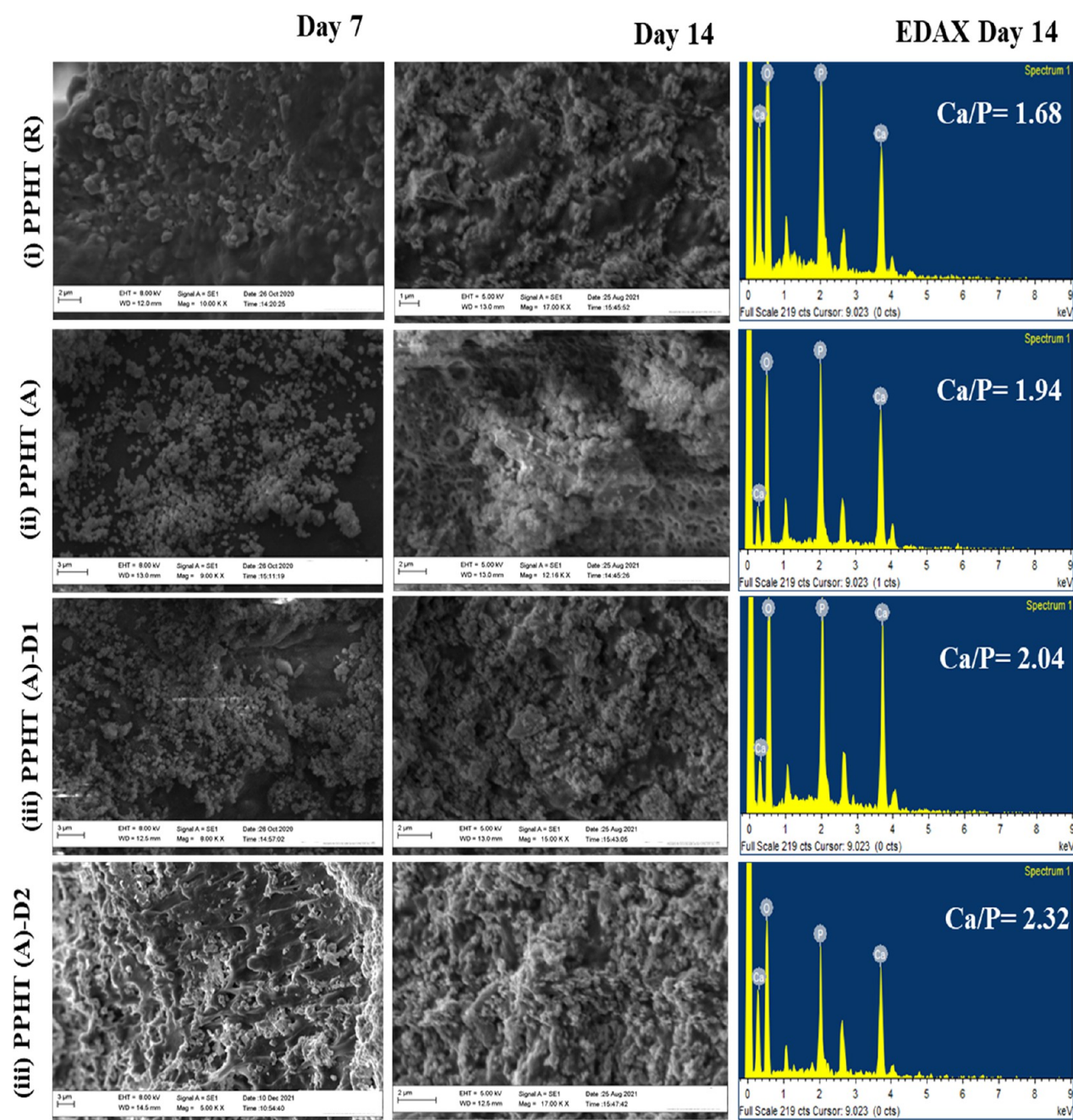
Figure 6. Macroscopic images of biomineralized PLA:PVA/HAP:TiO$_2$ fibrous scaffolds with and without CEM after immersion in SBF medium for 7 and 14 days.

4.5. *In Vitro* Degradation Profile and Porosity Measurement. As discussed in the contact angle measurement, all the scaffolds showed a hydrophilic nature, which may lead to an increase in the biodegradation rate. The *in vitro* biodegradation rates of PLA and PVA nanofibers are well-defined by many studies related to bone regeneration applications. Immersion of PLA:PVA/HAP:TiO$_2$ with and without CEM drug composites in SBF solution was evaluated for 7, 14, and 28 days and is shown in Figure 5. The substantial change or weight loss of biodegraded scaffolds was evaluated by weight ratio calculation. The polymers in the composite may degrade by chemical attack (oxidation), which involves the cleavage of carboxyl groups, depolymerization, and cation species in the testing medium.[42]

Salahuddin *et al.* reported that the PLA polymer in the human system could degrade into a nontoxic monomer (lactic acid), carbon dioxide, and water via chain disruption, which are excreted in urine via the Krebs cycle.[43] Moreover, Eslami *et al.* investigated the degradation rate of the poly(lactic-*co*-glycolic acid)PLGA/TiO$_2$ composite in SBF solution and the effect of TiO$_2$ on the composite. The study proposed that the dispersion of TiO$_2$ in the matrix could increase the surface/volume ratio and crystallinity of the composite, thereby decreasing the interaction of water molecules with ester bonds in PLA.[44] Hence, titanium dioxide in the nanofibers will increase the hydrophilicity and surface area; as a result, it decreases the degradation rate of the nanofibers.
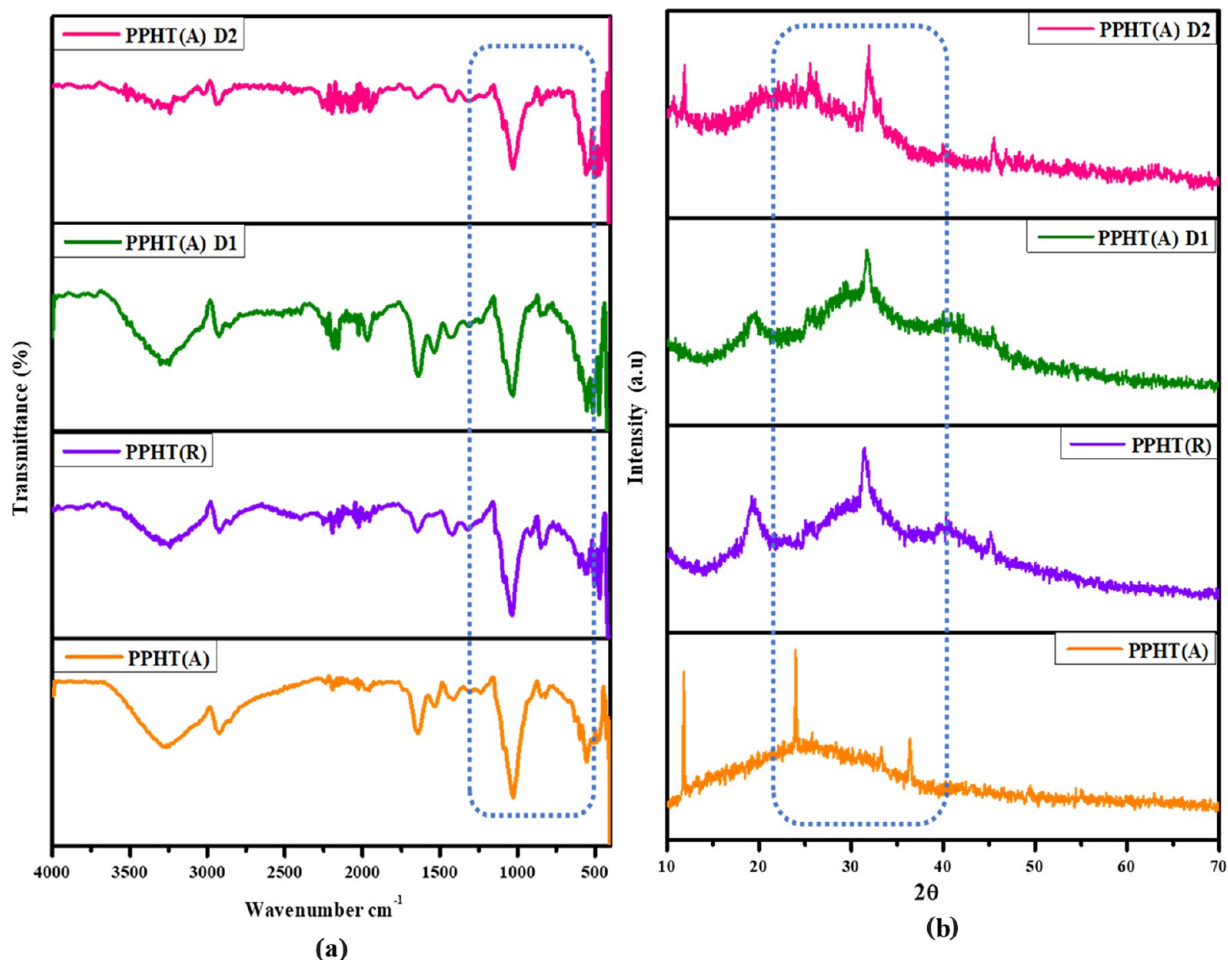
Figure 7. (a,b) FTIR and XRD patterns of biomineralized PLA:PVA/HAP:TiO$_2$ (rutile and anatase) nanofibers and CEM-loaded PLA:PVA/HAP:TiO$_2$ nanofibers after 14 days of incubation.

In addition, after 14−28 days, the alkaline ions of hydroxyapatite in the nanofibrous scaffold started to degrade along with calamitous disintegration of PLA:PVA. When compared to drug-embedded scaffolds, the significant increase was observed in the degradation rate; this might be due to the interaction of carbonyl groups belonging to the active site of the drug molecule (which is in accordance with FTIR results) with hydroxyl groups of HAP:TiO$_2$ (*i.e.*, TiO$_2$ generates hydroxy ions after a prolonged period of SBF incubation). Lieberman and Vemuri reported that, in a biological environment, most antibiotic drugs undergo hydrolytic degradation of carbonyl groups such as esters, lactones, amides, carbamates, imides, and lactams into imines.[45] Determination of porosity was analyzed using a liquid displacement method based on our previous study.[26] The porosities of fabricated PPHT(R), PPHT(A), PPHT(A)-D1, PPHT(A)-D2 nanofibers were 76.34 ± 1.65, 78.92 ± 1.73, 82.67 ± 1.70, and 85.89 ± 1.09%, respectively. The porosity of the nanofiber increased with the addition of the CEM drug. The higher porosity of the CEM-loaded nanofibers (PPHT-(A)-D2) could promote oxygen exchange and supply nutrients, which is also in accordance with Shahverdi *et al.*[46] This study depicted that the higher mechanical strength and density of the drug-loaded nanofibers could yield a higher porosity, which might be due to the decrease in compactness in the inclusion of the cephalexin drug. Owing to this, the drug-embedded

anatase phase showed more degradation and porosity than the rutile crystalline phase in the nanofibers.

4.6. Bioactivity Property of Nanofibers. The bioactivity (*i.e.*, osteoconductivity in the SBF) was assessed by detecting the bone forming ability on PPHT(R), PPHT(A), and CEM-loaded PPHT(A)-D1 and PPHT(A)-D2 (*i.e.*, biological apatite formation in between the scaffold and ECM interface). The scaffolds under investigation were incubated in SBF solution for a period of 14 days. The surfaces of the incubated samples at 14 days were investigated to confirm the apatite formation by using SEM (Figure 6), FTIR, and XRD (Figure 7,b), indicating the osteoconductive property in physiological conditions.

4.6.1. SEM Analysis. SEM images (Figure 6) show the microstructure of biomineralized nanofibrous scaffolds after 7 and 14 days of immersion in the SBF; the formation of apatite nanoparticles on the surface was clearly seen in the spectra. The formed apatite particles are observed with a spherical-like orientation with agglomeration. During the deposition, the calcium and phosphorus ions in the scaffold increase the rate of formation of apatite with respect to the reaction time. The effect of phase formation of TiO$_2$ with HAP in the ratio of 3:2 (HAP:TiO$_2$) does not show any significant difference in rutile and anatase sheets. However, there is a difference in EDAX spectra where the rutile composition resulted in a Ca/P value less than the anatase composition. The molar ratios of Ca/P of the PPHT(R), PPHT(A), PPHT(A)-D1, and PPHT(A)-D2
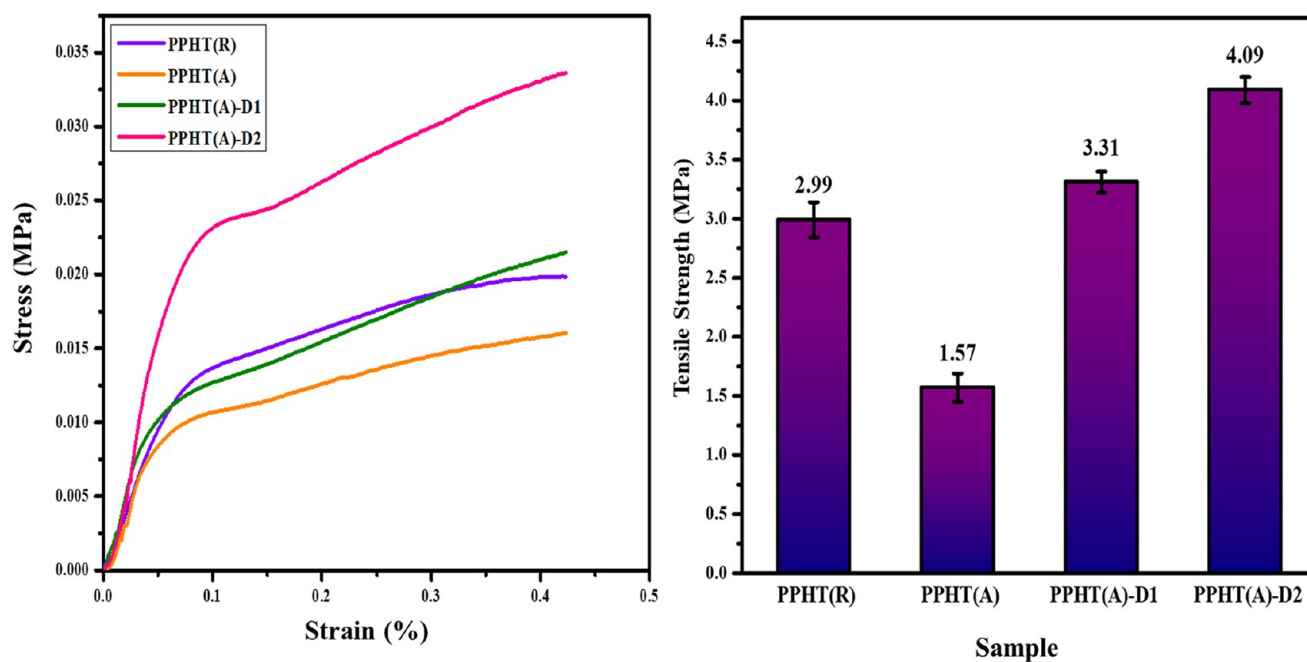
Figure 8. Tensile strengths of PLA:PVA/HAP:TiO$_2$ (rutile and anatase) nanofibers and CEM-loaded PLA:PVA/HAP:TiO$_2$ nanofibers.

nanofibers were 1.68, 1.94, 2.05, and 2.32, respectively. This result is in accordance with Roach *et al.*, where anatase enhances more apatite nucleation than that of rutile, which may be due to the crystalline lattice difference between the two phases.[47] As predictable, PPHT(A)-D2 shows more deposition than PPHT(R)-D1, which may be comparatively due to the porosity created by the addition of drug molecules via covalent bonding. All the Ca/P ratios revealed better apatite formation similar to the natural bone, which makes the scaffold a biomimetic composite. However, the active group of CEM via a covalent linkage with the polymeric composite reinforces the adsorption of positive Ca^{2+} and carboxyl ions through electrostatic interactions in the SBF.[48] Indeed, the presence of HAP with the drug supplies oxygen-containing hydroxy groups, which may trigger the nucleation process. The SEM and EDAX findings of biological apatite formation are further examined using XRD and FTIR results.

4.6.2. FTIR and XRD Analysis. Figure 7 displays the characteristic bands obtained for SBF-immersed nanofibers at 14 days; the peak at 550 cm^{-1} was assigned to the formation of phosphate bending, and those at 1200−900 (v_1 and v_3) and 700−450 cm^{-1} (v_2 and v_4) were assigned to the four vibrational modes of phosphate ions. As observed in all the FTIR spectra, OH stretching of the biomineralized calcium phosphate lattice was found at 3572 cm^{-1}.[49] Figure 7b shows the X-ray diffraction pattern of nanofibers after 14 days of incubation in SBF solution; broad prominent crystalline peaks at 25.8 and 31.8° indicate the formation of a nonstoichiometric apatite layer.[50] The characteristic peaks at 28, 42, and 47° indicate the presence of a less crystalline apatite phase or the mixture of ACP (amorphous calcium phosphate) in PPHT(A). As observed from the 14-day immersion results, peaks of the ACP phase indicate the dense formation of apatite on the surface of the nanofibers. The presence of TiO$_2$ as the rutile phase was found to improve the nucleation of calcium phosphate crystals on the surface.

Zhang *et al.* investigated the bioactivity of amorphous calcium phosphate/HAP/PLA composite nanofibers; the presence of calcium phosphate in the nanofibers triggered the nucleation process in SBF immersion.[51] This phenomenon depicted that calcium phosphate (HAP) in the composite could promote apatite deposition. More apatite formation was found on the drug-embedded nanofibers where the reactive groups of CEM drugs may trigger the interactions with free ions of the unstable SBF. The resulting interactions may drive the adsorption of calcium and phosphate in the SBF on the drug-embedded PLA:PVA/HAP:TiO$_2$ nanofibers. From XRD spectra, it was observed that rutile phase-incorporated scaffolds have more biomineralization capacity; the anatase phase with different concentrations of CEM loading leads to excellent biomineralization capacity in terms of more apatite growth. The above biomineralization results impart the bioactivity of the scaffold, which has the ability to form new bones.

4.7. Mechanical Property of the CEM-Loaded and Unloaded Nanofibers. The mechanical strength of the electrospun scaffolds with and without CEM was evaluated using a tensile testing machine and is illustrated in Figure 8. The incorporation of HAP and TiO$_2$ would significantly increase the tensile strength of the PLA:PVA nanofibers wherein the elongation at break decreased. It was observed that the average elongation at break for the rutile phase of the titanium dioxide composite scaffold was found to be 35 ± 2.1, and that of the anatase phase of the titanium dioxide composite scaffold was 31 ± 3.7. For the drug-loaded scaffolds, the elongation at break was found to be increased to 45 ± 3.09 and 53 ± 2.77, respectively.

Karimi *et al.* reported that the tensile strength of the nanofibers increased with the addition of hydrophilic TiO$_2$ nanoparticles. The greater hydroxyl groups in PVA would strongly interact with TiO$_2$ and HAP particles in the composite and increase the rigidity of the nanofibers.[52] Similarly, Jaiswal *et al.* had also reported that the addition of ceramic to either HAP or TiO$_2$ could not only improve the mechanical property but also increase the frictional forces between the fibrous mesh.[53] However, the increase in the mass fraction of HAP/ TiO$_2$ increases the intermolecular hydrogen bonding with the
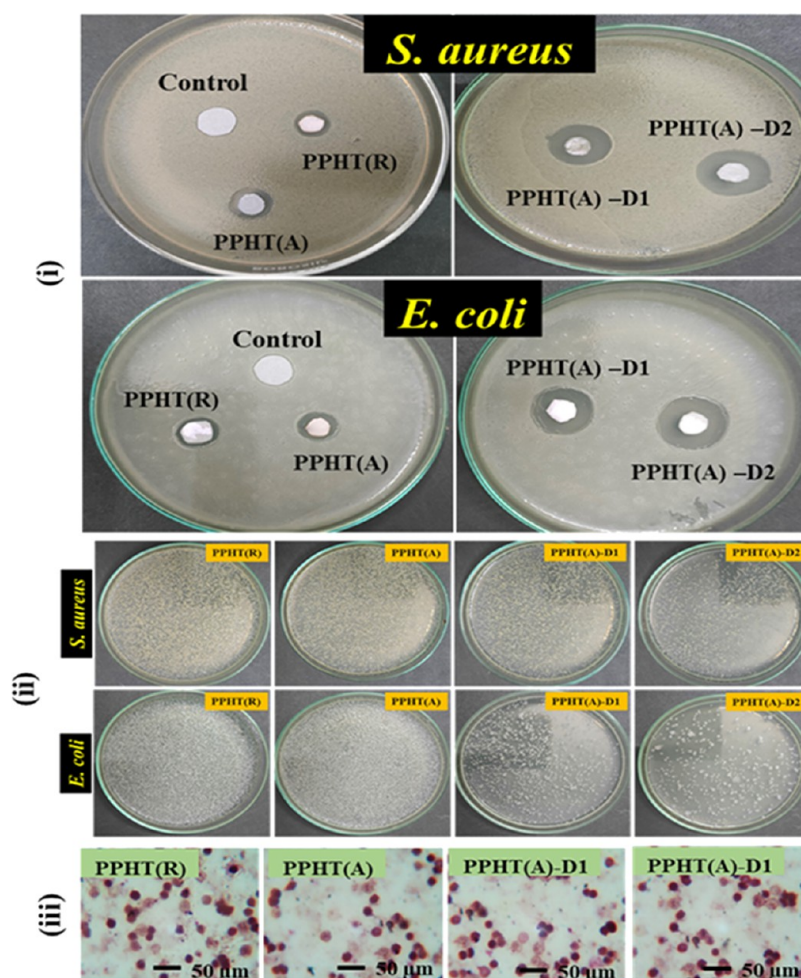
Figure 9. (i,ii) Antibacterial assessment by the qualitative disc diffusion method and the quantitative CFU method of CEM-loaded and unloaded PLA:PVA/HAP:TiO$_2$ nanofibrous scaffolds against *S. aureus* and *E. coli* and (iii) hemocompatibility assessment.

Table 2. Number of Counted Colonies and Respective CFU/mL for *S. aureus* and *E. coli*

plate ID	volume of plated culture	dilution	colony count (1 cm^2) [quartet]				mean	CFU/mL
			E. coli					
control	0.1 mL	1000	102	119	107	113	110	1.10
PPHT(R)	0.1 mL	1000	80	87	87	84	84.5	0.84
PPHT(A)	0.1 mL	1000	78	83	81	76	79.4	0.79
PPHT(A)-D1	0.1 mL	1000	47	50	52	46	48.7	0.48
PPHT(A)-D2	0.1 mL	1000	26	27	24	28	26.2	0.26
			S. aureus					
control	0.1 mL	1000	109	111	114	105	109	1.09
PPHT(R)	0.1 mL	1000	88	94	91	93	91.5	0.91
PPHT(A)	0.1 mL	1000	86	90	86	85	86.5	0.86
PPHT(A)-D1	0.1 mL	1000	65	71	64	60	65	0.65
PPHT(A)-D2	0.1 mL	1000	42	44	39	45	42.5	0.42

polymeric matrix PLA/PVA, which results in an increase in the crystallinity of the composite nanofibers by enhancing the mechanical stability. From this study, it was evidenced that the incorporation of the CEM drug thereby lowers the elasticity of nanofibers by creating electrostatic forces during the electro-spinning process or may also be due to the covalent bonding or intermolecular interactions between CEM with PLA:PVA espun solution. The tensile strengths of PPHT(R), PPHT(A), PPHT(A)-D1, and PPHT(A)-D2 were 2.99 ± 0.15, 1.57 ± 0.12, 3.21 ± 0.09, and 4.09 ± 0.11 MPa, respectively. Probably,

the interaction between the higher amount of the CEM drug and the polymeric matrix has been the major reason for the considerable increase in the mechanical property.

4.8. Antibacterial Evaluation and Hemocompatibility. The antibacterial activity of the drug-loaded nanofibers was tested against *S. aureus* and *E. coli*, with the zone of inhibition shown in Figure 9(i) and the CFU method shown in Figure 9(ii). It can be perceived that HAP/TiO$_2$ alone could not inhibit the growth of bacterial strains effectively. Seyedmajidi *et al.* depicted that the release of active oxygen groups from HAP
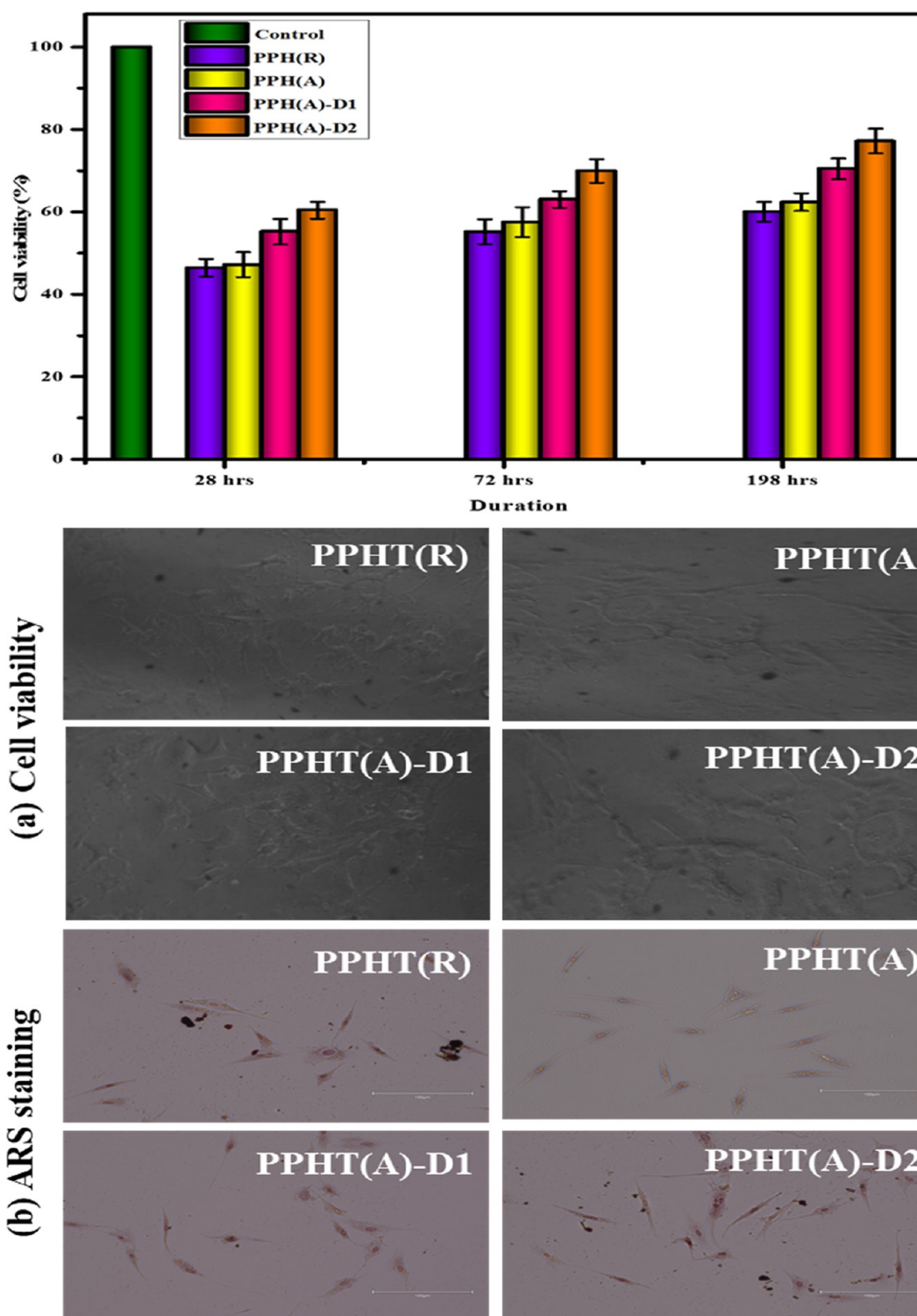
Figure 10. (a,b) *In vitro* cell viability and cell differentiation of CEM-loaded and unloaded PLA:PVA/HAP:TiO$_2$ nanofibers using the MG63 cell line.

could exhibit antibacterial potency only when the particle size of HAP ranges within the nanoscale level and reduced on increasing the sintering temperature of HAP.[54] The higher inhibition zone was found in the scaffolds that have a higher drug concentration. Further, it was observed that the inclusion of CEM increased the antibacterial efficacy in both qualitative and quantitative assessment, which might be due to the burst release of the drug from the scaffold. However, with the

addition of HAP and TiO$_2$ into the composite nanofibers, no obvious change was observed with respect to the inhibition zone, which is in accordance with Wang *et al.*[55] This study proposed that HAP has a low antibacterial activity in the absence of any therapeutic agents and could result in a prolonged antibacterial effect in the presence of a drug. From Figure 9(ii) and Table 2, the number of Gram-positive and Gram-negative bacterial colonies on the cultured medium was

found to be reduced in the presence and increase in the CEM drug concentration (*i.e.*, PPHT(R) < PPHT(A) < PPHT(A)-D1 < PPHT(A)-D2).

Aygen *et al.* anticipated that CEM is used as a powerful antibiotic agent; it can deactivate bacteria by binding with inner bacterial cell walls (*i.e.*, penicillin-binding properties, PBP).[56] Akhlaghi *et al.* proposed four antibacterial mechanisms of beta-lactam antibiotic inhibition: (i) an increase in the PBP active sites lowering the surface affinity of the antibiotic, (ii) a change in proteins of Gram-negative bacteria due to beta-lactam diffusion, (iii) a change in the periplasm of Gram-negative pathogens due to a multicomponent drug efflux system, and (iv) a change in production of beta-lactamases.[57] Therefore, the antibacterial results imply that the CEM antibiotic drug-embedded nanofibers could resist bacteria effectively. Furthermore, the interaction of blood cells and biomaterials (drug-loaded nanofibers) may lead to cellular reactions after grafting and create undesirable inflammation.

The hemolytic assay of CEM-loaded nanofibers revealed (Figure 9(iii)) that the varied hemolysis value was lower than 5%, which is quite similar to the negative PBS control. The OD values of rutile and anatase phases are similar, while drug-loaded samples showed relatively higher values. These hemolysis results suggested that all the samples including drug-loaded samples have a quite low hemolytic effect. The hemolytic values were found to be 0.71, 0.74, 0.90, and 1.23% for PPHT(R) < PPHT(A) < PPHT(A)-D1 < PPHT(A)-D2. Thus, the hemolysis assay of biomaterials could indicate damage of blood cells, which can decrease the side effects such as thrombus formation. The hemolysis value of the prepared scaffolds was found to be less than the standard criterion of 5%, confirming the hemocompatibility of the bioimplant.

4.9. *In Vitro* Cytocompatibility and Alizarin Red Staining Assessment.

Figure 10 shows the *in vitro* cell viability assessment by the MTT assay of CEM-loaded and unloaded PLA:PVA/HAP:TiO$_2$ nanofibrous scaffolds using the MG63 cell line for 28, 72, and 198 h. Results in Figure 10 have demonstrated that the ratio of HAP/TiO$_2$ to PLA/PVA did not show any inhibitory effect on the cytocompatibility aspects of the prepared scaffolds. The cell number and attachment were found to be increased with the increase in culture time from 28 to 198 h with respect to the composition of the fibrous mat. The cells seeded on anatase-based scaffolds with and without the drug have a less significant difference in the proliferation rate at 28 h. The PLA:PVA/HAP:TiO$_2$(rutile) showed the least cell viability rate (60.02 ± 2.39%) compared to other groups of PLA:PVA/HAP:TiO$_2$(anatase) sheets (62.37 ± 2.13) after 198 h. Moreover, the cell distribution and viability on the nanofibers were observed using microscopy after 198 days of culture, where all the cells are found to be alive even in CEM drug-embedded nanofibers. Lv *et al.* reported that anatase has more active hydroxy groups and cell binding sites on the surface, which ensues preosteoblast adhesion, spreading, and proliferation compared to the rutile phase.[58] In our previous study,[59] cell proliferation with less or no dead cells was observed on the composite nanofiber with the addition of the CEM drug. The drug concentrations of PLA:PVA/HAP:TiO$_2$(anatase)/D1 and PLA:PVA/HAP:-TiO$_2$(anatase)/D2 sheets recorded values of 70.44 ± 2.54 and 77.17 ± 3.01% of cell viability, which confirmed the nontoxicity of the CEM drug toward osteoblast cells.

Lin et el. had investigated the osteogenic activity of anatase and rutile phases of TiO$_2$; since both are hydrophilic, the cell

viability and adhesion of cells were found to be less in rutile than in anatase.[60] However, TiO$_2$ absorbs water molecules; the distance between active oxygen atoms with oxygen vacancy sites of the anatase phase is less than that of the rutile structure.[61] Hence, the lower distance of anatase can decrease the dissociation energy and facilitates hydrogen bonding to enhance hydrophilicity. Studies reported that TiO$_2$ nanofibers absorb water molecules to form Ti−OH, which could generate electrostatic interactions with active/binding sites of cells to promote osteoblast differentiation.[62,63] Similarly, the study by Saha *et al.* depicted that the surface chemistry of TiO$_2$ (*i.e.*, hydrophilicity due to surface −OH groups) highly impacted cell adhesion and proliferation.[63] According to the present study, the presence of the anatase phase showed better cell viability than the rutile phase on the composite nanofibers. Moreover, a large number of live cells were observed on the CEM-loaded PLA:PVA/HAP:TiO$_2$(anatase)/D2 sheet, which could promote live cell viability.

Furthermore, the calcium nodules of MG63 cells can be detected via Alizarin red S staining, where red nodules in Figure 10b represent the cellular calcification on the prepared scaffolds after 14 days. As observed, the CEM drug-loaded and unloaded nanofibers showed significant differences, which might be due to the effect of the incorporated CEM drug. All the scaffolds showed the formation of calcium nodules, and PLA:PVA/HAP:TiO$_2$(anatase)/D2 nanofibers showed more red areas. The addition of CEM enhanced the calcification process (calcium deposition) with respect to the promotion of osteoblastic differentiation, which was in agreement with the MTT assay. Lin *et al.* had suggested that incorporation of a drug in the nanofibers could stimulate osteogenic differentiation of MG63 cells.[65] Hence, in this current work, the CEM-loaded PLA:PVA/HAP:TiO$_2$ scaffolds did not show any negative effect on MG63 cells and can be considered as good candidates for biomaterial applications.

4.10. *In Vitro* Drug Release.

The cephalexin drug release was analyzed by using a UV−visible spectrophotometer at a wavelength of 261 nm at different intervals of 0−24 h for 8 days as shown in Figure 11. The diverse release of the drug was observed from CEM-loaded PLA:PVA/HAP:TiO$_2$ (*i.e.*, PPHT-(R) and PPHT(A)) scaffolds (in which drug inclusion was performed into scaffolds via physical adsorption) and CEM-functionalized PLA:PVA/HAP:TiO$_2$(anatase)/D scaffolds (PPHT(A)-D1 and PPHT(A)-D2), in which drug molecules were covalently bonded with the polymer/ceramic composite. Figure 11 shows that the drug release curves from the physically loaded scaffold matrix resulted in an initial burst release of 50%, which is mainly attributed to the drug adsorbed on the surface of the nanofiber up to 8 h. The sustained drug release was observed from the PPHT(R) and PPHT(A) scaffolds where 100% of the loaded drug has been completely released after a period of 8 days. The drug release curves of CEM-functionalized PPHT(A)-D1 and PPHT(A)-D2 scaffolds showed an initial burst release of 70%, which may be owing to the drug bonded on the surface of nanofibrous matrices.

The drug release from PPHT(A)-D1 and PPHT(A)-D2 has attained 100% along with the degradation of the composite matrix. Patrojanasophon *et al.* anticipated that highly aligned nanofibers can release the drug molecules from the matrix via diffusion.[64] Hypothetically, hydrophobic PLA in the matrix could not take part in dissolution, whereas the inclusion of PVA in the matrix can facilitate drug release. In this work,
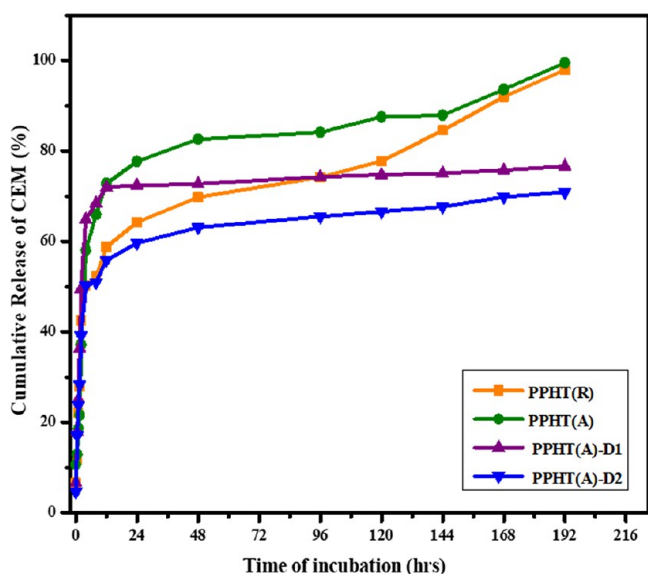
Figure 11. *In vitro* drug release profile of CEM-loaded PLA:PVA/HAP:TiO$_2$ (rutile and anatase) nanofibers via physical adsorption and CEM-embedded PLA:PVA/HAP:TiO$_2$ nanofibers.

covalently bonded drug molecules could be released through the interfibrous space created when PVA degrades along with HAP/TiO$_2$. Subsequently, only 75% of the drug has been released from PPHT(A)-D1 and PPHT(A)-D2, which might be due to the strong interaction of the drug with the polymeric fibrous system. Eventually, a higher concentration of the drug from PPHT(A)-D2 showed a better releasing ability than the PPHT(A)-D1 scaffold. On comparing, the physically incorporated drug scaffolds showed faster release, which may be due to weaker molecular interactions between the drug and the active polymeric surface of the scaffolds. Such an electrostatically bonded surface can exclude more initial burst release than covalently modified scaffolds, where the release is found to be static unless the polymer degrades.

Sun *et al.* had proposed that drug-loaded fibers are released in PBS medium via a surface diffusion process through interconnected pores caused by the degradation process.[66] However, the drug release profile of two different patterned scaffolds showed zero-order kinetics in a sustained release manner, and the functional scaffold resulted in constant release at a prolonged period.

5. CONCLUSIONS

In this work, we have fabricated a novel PLA:PVA/HAP:TiO$_2$ scaffold encapsulated with the CEM drug; the results denote the effective bone bonding ability to treat bone-related infections. The ratios of HAP:TiO$_2$ and PLA:PVA had improved the mechanical and biological performance of the scaffolds.

- The SEM microstructure of hydrophilic PLA:PVA/HAP:TiO$_2$ encapsulated with the CEM drug revealed that the presence of CEM in the scaffold had altered the fiber diameter with an increased tensile strength.
- The higher hydroxyl groups in the anatase phase of TiO$_2$ in the nanofibrous surface had promoted the cell viability and also created an electrostatic interaction with free ions in the SBF solution to form a dense apatite layer.

- The higher porosity of covalently loaded CEM in the PPHT(A)-D2 composite had shown more apatite formation and prolonged drug release compared to CEM-incorporated nanofibers via physical adsorption. The antibacterial efficacy and osteogenic differentiation increased with the addition of the CEM drug into the composite nanofibers.
- On comparing both PPHT(A)-D1 and PPHT(A)-D2 nanofibers, the higher concentration of the drug in the matrix (*i.e.*, 5 mg/mL) had shown better efficacy in all biological evaluations.
- Thus, we proposed that the covalently loaded or chemically modified CEM-incorporated PLA:PVA/HAP:TiO$_2$ nanofiber bioscaffolds for bone regeneration and prolonged antibiotic release could prevent bone-related infections.

■ AUTHOR INFORMATION

Corresponding Author

Vijayalakshmi Uthirapathy − *Department of Chemistry, School of Advanced Sciences, Vellore Institute of Technology, Vellore, Tamil Nadu 632014, India;* ⊙ orcid.org/0000-0003-0727-4277; Email: vijayalakshmi.u@vit.ac.in

Authors

Rama Murugapandian − *Department of Chemistry, School of Advanced Sciences, Vellore Institute of Technology, Vellore, Tamil Nadu 632014, India*

Simona Clement − *Department of Chemistry, Virginia Commonwealth University, Richmond, Virginia 23284, United States*

Complete contact information is available at:
https://pubs.acs.org/10.1021/acsomega.2c07701

Notes

The authors declare no competing financial interest.

■ REFERENCES

(1) Zhen, W.; Yichuan, W.; Jiaqi, Y.; Keshi, Z.; Feng, L.; Lei, X.; Lianfu, D.; Zhenpeng, G.; Wenguo, C.; Hongbo, Z. Pharmaceutical electrospinning and 3D printing scaffold design for bone regeneration. *Adv. Drug Delivery Rev.* **2021**, *174*, 504−534.

(2) Bharadwaz, A.; Jayasuriya, A. C. Recent trends in the application of widely used natural and synthetic polymer nanocomposites in bone tissue regeneration. *Mater. Sci. Eng. C* **2020**, *110*, 110698.

(3) Priyadarshini, B.; Ramya, S.; Shinyjoy, E.; Kavitha, L.; Gopi, D.; Vijayalakshmi, U. Structural, morphological and biological evaluations of cerium incorporated hydroxyapatite sol−gel coatings on Ti−6Al−4V for orthopaedic applications. *J. Mater. Res. Technol.* **2021**, *12*, 1319−1338.

(4) Mitra, J.; Tripathi, G.; Sharma, A.; Basu, B. Scaffolds for bone tissue engineering: role of surface patterning on osteoblast response. *RSC Adv.* **2013**, *3*, 11073−11094.

(5) Fathi, M.; Akbari, B.; Taheriazam, A.; Sodagar, A. Surface functionalization of Titania Nanotubes arrays and vancomycin

controlled release using Silk Fibroin Nanofibers coating. *J Drug Deliv Sci Technol.* **2022**, *71*, 103320.

(6) Farokhi, M.; Mottaghitalab, F.; Samani, S.; Shokrgozar, M. A.; Kundu, S. C.; Reis, R. L.; Fatahi, Y.; Kaplan, D. L. Silk fibroin/hydroxyapatite composites for bone tissue engineering. *Biotechnol. Adv.* **2018**, *36*, 68−91.

(7) Ingole, V. H.; Ghule, S. S.; Vuherer, T.; Kokol, V.; Ghule, A. V. Mechanical Properties of Differently Nanostructured and High-Pressure Compressed Hydroxyapatite-Based Materials for Bone Tissue Regeneration. *Minerals* **2021**, *11*, 1390.

(8) Chellappa, M.; Vijayalakshmi, U. In-situ fabrication of zirconium−titanium nano-composite and its coating on Ti-6Al-4V for biomedical applications. *IET Nanobiotechnol.* **2017**, *11*, 83−90.

(9) Khan, M. U. A.; Haider, S.; Shah, S. A.; Abd Razak, S. I.; Hassan, S. A.; Kadir, M. R.; Haider, A. Arabinoxylan-co-AA/HAp/TiO$_2$ nanocomposite scaffold a potential material for bone tissue engineering: An *in vitro* study. *Int. J. Biol. Macromol.* **2020**, *151*, 584−594.

(10) Stipniece, L.; Narkevica, I.; Sokolova, M.; Locs, J.; Ozolins, J. Novel scaffolds based on hydroxyapatite/poly (vinyl alcohol) nanocomposite coated porous TiO2 ceramics for bone tissue engineering. *Ceram. Int.* **2016**, *42*, 1530−1537.

(11) Meenashisundaram, G. K.; Nai, M. H.; Almajid, A.; Khalil, K. A.; Abdo, H. S.; Gupta, M. Effects of TiO$_2$ powder morphology on the mechanical response of pure magnesium: 1D nanofibers versus 0D nanoparticulates. *J. Alloys Compd.* **2016**, *664*, 45−58.

(12) Rama, M.; Ashwin, S. S.; Lokesh, V.; Aqza Elza, J. Vijayalakshmi, U; A Review on Nanofibrous Scaffolding Technique for Potential Tissue Engineering Applications. *Trends Biomater. Artif. Organs.* **2022**, *36*, 27−37.

(13) Ferreira, F. V.; Otoni, C. G.; Lopes, J. H.; De Souza, L. P.; Mei, L. H.; Lona, L. M.; Lozano, K.; Lobo, A. O.; Mattoso, L. H. Ultrathin polymer fibers hybridized with bioactive ceramics: A review on fundamental pathways of electrospinning towards bone regeneration. *Mater. Sci. Eng. C* **2021**, *123*, 111853.

(14) Islam, M. S.; Ang, B. C.; Andriyana, A.; Afifi, A. A review on fabrication of nanofibers via electrospinning and their applications. *SN Appl. Sci.* **2019**, *1*, 1248−1252.

(15) Mary Stella, S.; Vijayalakshmi, U. Influence of chemically modified Luffa on the preparation of nanofiber and its biological evaluation for biomedical applications. *J. Biomed. Res. Part A.* **2019**, *107A*, 610−620.

(16) Tyler, B.; Gullotti, D.; Mangraviti, A.; Utsuki, T.; Brem, H. Polylactic acid (PLA) controlled delivery carriers for biomedical applications. *Adv. Drug Delivery Rev.* **2016**, *107*, 163−175.

(17) Teixeira, M. A.; Teresa, P.; Amorim, M. T.; Felgueiras, H. P. Poly (vinyl alcohol)-based nanofibrous electrospun scaffolds for tissue engineering applications. *Polymer* **2020**, *12*, 7.

(18) Kundu, D.; Banerjee, T. Development of microcrystalline cellulose based hydrogels for the *in vitro* delivery of Cephalexin. *Heliyon* **2020**, *6*, 1.

(19) Pereira, P.; Serra, A. C.; Coelho, J. F. Vinyl Polymer-based technologies towards the efficient delivery of chemotherapeutic drugs. *Prog. Polym. Sci.* **2021**, *121*, 101432.

(20) Shuford, G. M. Concentrations of cephalexin in mandibular alveolar bone, blood, and oral fluids. *J. Am. Dent. Assoc.* **1939**, *99*, 47−50.

(21) Ploger, G. F.; Quizon, P. M.; Abrahamsson, B.; Cristofoletti, R.; Groot, D. W.; Parr, A.; Langguth, P.; Polli, J. E.; Shah, V. P.; Tajiri, T.; Mehta, M. U. Biowaiver monographs for immediate release solid oral dosage forms: cephalexin monohydrate. *J. Pharm. Sci.* **2020**, *109*, 1846−1862.

(22) Kataria, K.; Gupta, A.; Rath, G.; Mathur, R. B.; Dhakate, S. R. In vivo wound healing performance of drug loaded electrospun composite nanofibers transdermal patch. *Int. J. Pharm.* **2014**, *469*, 102−110.

(23) Rama, M.; Vijayalakshmi, U. Drug delivery system in bone biology: an evolving platform for bone regeneration and bone infection management. *Polym. Bull.* **2022**, 1−48.

(24) Hu, Z.; Das, S. K.; Yan, S.; You, R.; Li, X.; Luo, Z.; Li, M.; Zhang, Q.; Kaplan, D. L. Stability and biodegradation of silk fibroin/hyaluronic acid nerve conduits. *Composites, Part B* **2020**, *200*, 108222.

(25) Rama, M.; Vijayalakshmi, U. Influence of silk fibroin on the preparation of nanofibrous scaffolds for the effective use in osteoregenerative applications. *J. Drug Delivery Sci. Technol.* **2021**, *61*, 102182.

(26) Rama, M.; Vijayalakshmi, U. Biological and mechanical investigation of novel flax/silk protein-based nanofibrous scaffold for bone regeneration. *Prog. Nat. Sci.* **2022**, *32*, 443−455.

(27) Vijayalakshmi, U. Structural phase formation and in vitro bioactivity evaluations of strontium phosphosilicate for orthopedic applications. *J. Biomed. Mater. Res.* **2020**, *108*, 3286−3301.

(28) Khalil, A. A.; Zawrah, M. F.; Saad, E. A.; Badr, H. A. Synthesis and properties of hydroxyapatite nanorods. *InterCeram* **2015**, *64*, 358−362.

(29) Vijayalakshmi, U.; Chellappa, M.; Anjaneyulu, U.; Manivasagam, G.; Sethu, S. Influence of coating parameter and sintering atmosphere on the corrosion resistance behavior of electrophoretically deposited composite coatings. *Mater. Manuf. Processes* **2016**, *31*, 95−106.

(30) Zhao, Y.; Nie, L.; Yang, H.; Song, K.; Hou, H. Tailored fabrication of TiO$_2$/In$_2$O$_3$ hybrid mesoporous nanofibers towards enhanced photocatalytic performance. *Colloids Surf., A* **2021**, *629*, 127455.

(31) Alsaiari, M. A.; Alhemiary, N. A.; Umar, A.; Hayden, B. E. Growth of amorphous, anatase and rutile phase TiO$_2$ thin films on Pt/TiO$_2$/SiO$_2$/Si (SSTOP) substrate for resistive random access memory (ReRAM) device application. *Ceram. Int.* **2020**, *46*, 16310−16320.

(32) Chellappa, M.; Thejaswini, B.; Vijayalakshmi, U. Biocompatibility assessment of SiO$_2$−TiO$_2$ composite powder on MG63 osteoblast cell lines for orthopaedic applications. *IET Nanobiotechnol.* **2017**, *11*, 77−82.

(33) Lukong, V. T.; Mouchou, R. T.; Enebe, G. C.; Ukoba, K.; Jen, T. C. Deposition and characterization of self-cleaning TiO$_2$ thin films for photovoltaic application. *Mater. Today: Proc.* **2022**, S63.

(34) Takai, Z. I.; Mustafa, M. K.; Sekak, K. A.; AbdulKadir, H. K.; Asman, S.; Idris, A.; Mohammad, J. Fabrication, characterization and X-band microwave absorption properties of PAni/Fe$_3$O$_4$/PVA nanofiber composites materials. *Arab. J. Chem* **2020**, *13*, 7978-89.

(35) Prasad, A.; Bhasney, S. M.; Sankar, M. R.; Katiyar, V. Fish scale derived hydroxyapatite reinforced poly (lactic acid) polymeric bio-films: possibilities for sealing/locking the internal fixation devices. *Mater. Today: Proc.* **2017**, *4*, 1340−1349.

(36) Rezk, A. I.; Bhattarai, D. P.; Park, J.; Park, C. H.; Kim, C. S. Polyaniline-coated titanium oxide nanoparticles and simvastatin-loaded poly (ε-caprolactone) composite nanofibers scaffold for bone tissue regeneration application. *Colloids Surf., B* **2020**, *192*, 111007.

(37) Haider, A.; Haider, S.; Kang, I.-K. A comprehensive review summarizing the effect of electrospinning parameters and potential applications of nanofibers in biomedical and biotechnology. *Arab. J. Chem.* **2018**, *11*, 1165−1188.

(38) Yu, J.; Zhao, X.; Yu, J.; Zhong, G.; Han, J.; Zhao, Q. The grain size and surface hydroxyl content of super-hydrophilic TiO$_2$/SiO$_2$ composite nanometer thin films. *J. Mater. Sci. Lett.* **2001**, *20*, 1745−1748.

(39) Niemczyk-Soczynska, B.; Gradys, A.; Sajkiewicz, P. Hydrophilic surface functionalization of electrospun nanofibrous scaffolds in tissue engineering. *Polymer* **2020**, *12*, 636.

(40) Cui, Z.; Zheng, Z.; Lin, L.; Si, J.; Wang, Q.; Peng, X.; Chen, W. Electrospinning and crosslinking of polyvinyl alcohol/chitosan composite nanofiber for transdermal drug delivery. *Adv. Polym. Technol.* **2018**, *37*, 1917−1928.

(41) Mishra, P.; Gupta, P.; Pruthi, V. Cinnamaldehyde incorporated gellan/PVA electrospun nanofibers for eradicating Candida biofilm. *Mater. Sci. Eng. C* **2021**, *119*, 111450.

(42) Tamariz, E.; Rios-Ramírez, A. Biodegradation of medical purpose polymeric materials and their impact on biocompatibility. *Biodegrad.: Life Sci.* **2013**, *14*, 1−29.

(43) Salahuddin, N.; Abdelwahab, M.; Gaber, M.; Elneanaey, S. Synthesis and Design of Norfloxacin drug delivery system based on PLA/TiO$_2$ nanocomposites: Antibacterial and antitumor activities. *Mater. Sci. Eng. C* **2020**, *108*, 110337.

(44) Eslami, H.; Lisar, H.; Kashi, T. S.; Tahriri, M.; Ansari, M.; Rafiei, T.; Bastami, F.; Shahin-Shamsabadi, A.; Abbas, F. M.; Tayebi, L. Poly (lactic-co-glycolic acid)(PLGA)/TiO$_2$ nanotube bioactive composite as a novel scaffold for bone tissue engineering: *In vitro* and *in vivo* studies. *Biologicals* **2018**, *53*, 51−62.

(45) Lieberman, H; Vemuri, N. M. Chemical and Physicochemical Approaches to solve formulation problems. In *The Practice of Medicinal Chemistry.* Academic Press2015, 767−791, DOI: 10.1016/B978-0-12-417205-0.00032-8.

(46) Shahverdi, F.; Barati, A.; Salehi, E.; Arjomandzadegan, M. Biaxial electrospun nanofibers based on chitosan-poly (vinyl alcohol) and poly (ε-caprolactone) modified with CeAlO3 nanoparticles as potential wound dressing materials. *Int. J. Biol. Macromol.* **2022**, *221*, 736−750.

(47) Roach, M. D.; Williamson, R. S.; Blakely, I. P.; Didier, L. M. Tuning anatase and rutile phase ratios and nanoscale surface features by anodization processing onto titanium substrate surfaces. *Mater. Sci. Eng. C* **2016**, *58*, 213−223.

(48) Rajendran, A.; Pattanayak, D. K. Mechanistic studies of biomineralisation on silver incorporated anatase TiO$_2$. *Mater. Sci. Eng. C* **2020**, *109*, 110558.

(49) Cai, Q.; Xu, Q.; Feng, Q.; Cao, X.; Yang, X.; Deng, X. Biomineralization of electrospun poly (l-lactic acid)/gelatin composite fibrous scaffold by using a supersaturated simulated body fluid with continuous CO$_2$ bubbling. *Appl. Surf. Sci.* **2011**, *257*, 10109−10118.

(50) Das, I.; De, G.; Hupa, L.; Vallittu, P. K. Porous SiO$_2$ nanofiber grafted novel bioactive glass−ceramic coating: A structural scaffold for uniform apatite precipitation and oriented cell proliferation on inert implant. *Mater. Sci. Eng. C* **2016**, *62*, 206−214.

(51) Zhang, H.; Fu, Q. W.; Sun, T. W.; Chen, F.; Qi, C.; Wu, J.; Cai, Z. Y.; Qian, Q. R.; Zhu, Y. J. Amorphous calcium phosphate, hydroxyapatite and poly (D, L-lactic acid) composite nanofibers: electrospinning preparation, mineralization and *in vivo* bone defect repair. *Colloids Surf., B* **2015**, *136*, 27−36.

(52) Karimi, E.; Raisi, A.; Aroujalian, A. TiO$_2$-induced photo-cross-linked electrospun polyvinyl alcohol nanofibers microfiltration membranes. *Polymer* **2016**, *99*, 642−653.

(53) Jaiswal, A. K.; Chhabra, H.; Kadam, S. S.; Londhe, K.; Soni, V. P.; Bellare, J. R. Hardystonite improves biocompatibility and strength of electrospun polycaprolactone nanofibers over hydroxyapatite: A comparative study. *Mater. Sci. Eng. C* **2013**, *33*, 2926−2936.

(54) Seyedmajidi, S.; Rajabnia, R.; Seyedmajidi, M. Evaluation of antibacterial properties of hydroxyapatite/bioactive glass and fluorapatite/bioactive glass nanocomposite foams as a cellular scaffold of bone tissue. *J Lab Physicians.* **2018**, *10*, 265−270.

(55) Wang, J.; Cai, N.; Chan, V.; Zeng, H.; Shi, H.; Xue, Y.; Yu, F. Antimicrobial hydroxyapatite reinforced-polyelectrolyte complex nanofibers with long-term controlled release activity for potential wound dressing application. *Colloids Surf., A* **2021**, *624*, 126722.

(56) Aygün, B.; Akıncıoğlu, A.; Sayyed, M. I.; Karabulut, A. Investigation of some drug active substances able to protect against radiation damage with experimental and Monte Carlo calculations. *Radiat. Phys. Chem.* **2022**, *191*, 109850.

(57) Akhlaghi, N.; Najafpour-Darzi, G. Multifunctional metal-chelated phosphonate/Fe3O4 magnetic nanocomposite particles for defeating antibiotic-resistant bacteria. *Powder Technol.* **2021**, *384*, 1−8.

(58) Lv, L.; Li, K.; Xie, Y.; Cao, Y.; Zheng, X. Enhanced osteogenic activity of anatase TiO$_2$ film: Surface hydroxyl groups induce conformational changes in fibronectin. *Mater. Sci. Eng. C* **2017**, *78*, 96−104.

(59) Lin, G.-W.; Chen, J.-S.; Tseng, W.; Lu, F.-H. Formation of anatase TiO$_2$ coatings by plasma electrolytic oxidation for photocatalytic applications. *Surf. Coat. Int.* **2019**, *357*, 28−35.

(60) Sun, C.; Liao, T.; Lu, G. Q.; Smith, S. C. The role of atomic vacancy on water dissociation over titanium dioxide nanosheet: a density functional theory study. *J. Phys. Chem. C* **2012**, *116*, 2477−2482.

(61) Lin, D.-J.; Fuh, L.-J.; Chen, W.-C. Nano-morphology, crystallinity and surface potential of anatase on micro-arc oxidized titanium affect its protein adsorption, cell proliferation and cell differentiation. *Mater. Sci. Eng. C* **2020**, *107*, 110204.

(62) Chellappa, M.; Anjaneyulu, U.; Manivasagam, G.; Vijayalakshmi, U. Preparation and evaluation of the cytotoxic nature of TiO$_2$ nanoparticles by direct contact method. *Int. J. Nanomed.* **2015**, *10 Suppl 1*, 31−41.

(63) Saha, S.; Kumar, R.; Pramanik, K.; Biswas, A. Interaction of osteoblast-TiO$_2$ nanotubes *in vitro*: the combinatorial effect of surface topography and other physico-chemical factors governs the cell fate. *Appl. Surf. Sci.* **2018**, *449*, 152−165.

(64) Patrojanasophon, P.; Tidjarat, S.; Opanasopit, P.; Ngawhirunpat, T.; Rojanarata, T. Influence of nanofiber alignment on the release of a water-soluble drug from cellulose acetate nanofibers. *Saudi Pharm J.* **2020**, *28*, 1210−1216.

(65) Lin, P.; Zhang, W.; Chen, D.; Yang, Y.; Sun, T.; Chen, H.; Zhang, J. Electrospun nanofibers containing chitosan-stabilized bovine serum albumin nanoparticles for bone regeneration. *Colloids Surf., B* **2022**, *217*, 112680.

(66) Sun, Y.; Cheng, S.; Lu, W.; Wang, Y.; Zhang, P.; Yao, Q. Electrospun fibers and their application in drug controlled release, biological dressings, tissue repair, and enzyme immobilization. *RSC Adv.* **2019**, *9*, 25712−25729.